# Structural Connectivity Enriched Functional Brain Network using Simplex Regression with GraphNet

Mansu Kim<br/>¹, Jingxaun Bao², Kefei Liu¹, Bo-yong Park³, Hyunjin Park<br/><sup>4,5</sup>, and Li ${\rm Shen}^{1,\star}$ 

- $^{1}\,$  Department of Biostatistics, Epidemiology, and Informatics, University of Pennsylvania, USA
  - <sup>2</sup> School of Arts and Sciences, University of Pennsylvania, USA
- <sup>3</sup> McConnell Brain Imaging Centre, Montreal Neurological Institute, McGill University, Canada
- School of Electronic and Electrical Engineering, Sungkyunkwan University, Korea Center for Neuroscience Imaging Research, Institute for Basic Science, Korea li.shen@pennmedicine.upenn.edu

Abstract. The connectivity analysis is a powerful technique for investigating a hard-wired brain architecture as well as flexible, functional dynamics tied to human cognition. Recent multi-modal connectivity studies had the challenge of combining functional and structural connectivity information into one integrated network. In this paper, we proposed a simplex regression model with graph-constrained Elastic Net (Graph-Net) to estimate functional networks enriched by structural connectivity in a biologically meaningful way with a low model complexity. Our model constructed the functional networks using sparse simplex regression framework and enriched structural connectivity information based on GraphNet constraint. We applied our model on the real neuroimaging datasets to show its ability for predicting a clinical score. Our results demonstrated that integrating multi-modal features could detect more sensitive and subtle brain biomarkers than using a single modality.

**Keywords:** Structural connectivity  $\cdot$  functional connectivity  $\cdot$  simplex regression  $\cdot$  GraphNet  $\cdot$  depression

### 1 Introduction

Connectivity analysis is a powerful technique for investigating a hard-wired brain architecture as well as flexible functional dynamics tied to human cognition [16,

<sup>\*</sup> This work was supported by the National Institutes of Health [R01 EB022574] and National Science Foundation [IIS 1837964]. Data were provided by the Human Connectome Project, WU-Minn Consortium (Principal Investigators: David Van Essen and Kamil Ugurbil; 1U54MH091657) funded by the 16 NIH Institutes and Centers that support the NIH Blueprint for Neuroscience Research; and by the McDonnell Center for Systems Neuroscience at Washington University.

23]. Indeed, the whole-brain structural connectome can be measured via diffusion magnetic resonance imaging (dMRI) data through tractography algorithms by approximating structural wiring in white matter. Functional connectivity is constructed by measuring statistical associations of temporal coherence between different brain regions, and often computed from the resting-state functional MRI (rs-fMRI) data.

In the functional domain, various network modeling methods were introduced to measure the degree of coherence in the functional network [3, 14, 19], such as Pearson correlation (PearC), partial correlation (PartC), and graphical LASSO (GL). These approaches provided a novel perspective for understanding a large-scale functional organization of the brain, which was often used for distinguishing healthy and diseased brains in the studies of psychiatric and neurological disorders [2, 13, 20]. Unlike functional connectivity that infers statistical association, structural connectivity provides information of physical neuronal connections of the complex brain network, which can be used for identifying disrupted physical wiring between distinct brain regions. Recent multi-modal studies found that imaging features combining structural and functional connectivity information provided better imaging biomarkers for common diseases [21, 22], indicating the integration of multi-modal features may help detect more sensitive and subtle brain biomarkers than using a single modality alone.

Recently, some studies have proposed various sparse models to estimate brain networks from structural, functional and/or genomic data. Huang et al. proposed a sparse simplex model (Simplex) to build a brain network using whole brain gene expression data, but their methods did not consider spatial proximity and structural connectivity [7]. Pineda-Pardo et al. applied adaptive GL to estimate an MEG connectivity network guided by a structural connectivity network [15]. Li et al. proposed an ultra-weighted-LASSO approach to efficiently estimate functional networks by considering structural connectivity and derivatives of the temporal signal [10]. These methods incorporated the adaptive LASSO regularization approach to incorporate multi-modal information. However, if one node is linked to two highly connected regions, this approach tends to select only one of the two regions randomly, thus inadequate to capture all the signals.

To over these limitations, in this paper, we proposed a simplex regression model with graph-constrained Elastic Net (GraphNet) to estimate functional networks enriched by structural connectivity in a biologically meaningful way with low model complexity. Our major contributions are as follows: i) We designed a simplex regression model to build a functional network. ii) We extended the simplex regression model to include the GraphNet penalty to incorporate structural connectivity computed from dMRI data using a tractography algorithm. iii) We applied our proposed algorithm to the Human Connectome Project (HCP) database to demonstrate its ability to predict a clinical score and showed the promise of our algorithm compared with multiple competing methods.

### 2 Materials

### 2.1 Data description

We obtained neuroimaging (i.e., fMRI and dMRI) and genotyping datasets from the HCP database. Specifically, genetically unrelated, non-twins, non-Hispanic, white participants with full demographic information were considered in this study; see Table 1 for their characteristics. Of those, we randomly selected 100 participants and divided them into two groups (depression vs healthy) with equal size based on the Diagnostic and Statistical Manual of Mental Disorders 5th edition depression (DSM-dep) scores. Participants with a DSM-dep larger than 6 were classified as depression subjects, and the remaining participants were classified as healthy subjects [12]. The age, sex, and mini-mental state examination were matched between healthy and depression groups.

Healthy Depression p-value Number of subjects 50 50 \_ Age  $29.06 \pm 3.89$  $28.66 \pm 3.54$ 0.5925Sex M:28, F:22 M:24, F:26 0.4284DSM-dep  $0.66 \pm 0.47$  $8.44 \pm 2.22$ < 0.0001Mini-Mental State Examination  $29.16 \pm 0.91$  $28.86 \pm 1.16$ 0.1538

Table 1. Participant characteristics.

## 2.2 Data pre-processing

HCP database provided minimally pre-processed neuroimaging (i.e., rs-fMRI and dMRI) and genotyping datasets. For the rs-fMRI data, the CIFTI dense time series data in standard grayordinate space were obtained using the minimal pre-processing pipeline, which includes corrections for EPI distortions and head motion, registration to the T1-weighted data and subsequently MNI space, skull removal, and intensity normalization [5]. Then, the artifacts of head movement, white matter, cardiac pulsation, arterial, and large vein related contributions were removed by FMRIB's ICA-based X-noisifier (FIX) [17]. Finally, we averaged the vertex-wise time-series into parcel-level using HCP multi-modal parcellation atlas (HCP-MMP) [4]. We added 12 subcortical regions to the 360 cortical areas yielding a total of 372 brain regions.

The dMRI data were processed using a procedure similar to the one described by Kim et al. [8]. Head motion and eddy current were corrected and then probabilistic tractography was performed to build structural connectivity using FSL [18]. Graph nodes were defined by HCP-MMP atlas and the edges were defined using connection density between the nodes. Finally, the structural connectivity information was used as the constraint in our proposed approach described later.

### 3 Methods

### 3.1 Simplex representation

Herein, we used the boldface lowercase letter to denote a vector, and the boldface uppercase letter to denote a matrix. Specifically, given the datasets  $X \in \mathbb{R}^{n \times p}$ , where X corresponded to the pre-processed rs-fMRI data as described in Section 2.2., n denoted time points of rs-fMRI data, and p denoted number of brain regions. The sparse simplex learning model proposed by  $Huang\ et\ al.$  was originally proposed to construct the neuroanatomical and transcriptomic networks [7]. The model is defined as follows:

$$\tilde{\boldsymbol{\beta}}_i = \min_{\boldsymbol{\beta}_i} ||\boldsymbol{X}_{(:,i)} - \boldsymbol{X}_{(:,\neq i)} \boldsymbol{\beta}_i||_2^2 + \lambda ||\boldsymbol{\beta}_i||_1 \quad s.t. \quad \boldsymbol{\beta}_i \ge 0, \boldsymbol{\beta}_i^T \mathbf{1} = 1, \quad (1)$$

where  $X_{(:,\neq i)}$  is the matrix X with the i-th column (i.e., i-th region) removed,  $X_{(:,i)}$  is the i-th column of X,  $\beta_i$  is p-1 dimensional coefficient vector for the i-th brain region, and  $\geq$  denotes "componentwise larger than or equal to". One advantage of the simplex regression model is that the simplex constraint yields network edge weights (i.e., regression coefficients) that can be treated as probability values.

# 3.2 Functional brain network construction with simplex regression framework and GraphNet constraint

We herein proposed an algorithm for constructing functional network enriched by structural connectivity. Fig. 1 showed overall procedure of our approach. Specifically, we proposed a sparse simplex regression model penalized by Graph-Net penalty. GraphNet penalty, proposed by *Grosenick et al.*, has an advantage for integrating biological graph constraint, such as structural connectivity, by encouraging the coefficients to be similar between two highly connected nodes [6]. For example, when the structural connectivity between the *i*-th and *j*-th regions is high, the GraphNet penalty forces the corresponding coefficients to be similar. Additionally, the structural connectivity contains white matter fiber information, which is a good source for a biological constraint. Thus, we applied the GraphNet penalty on the sparse simplex regression model. The formula for the algorithm is defined as follows:

$$\tilde{\boldsymbol{\beta}}_{i} = \min_{\boldsymbol{\beta}_{i}} ||\boldsymbol{X}_{(:,i)} - \boldsymbol{X}_{(:,\neq i)} \boldsymbol{\beta}_{i}||_{2}^{2} + \lambda ||\boldsymbol{\beta}_{i}||_{1} + \lambda_{G} \boldsymbol{\beta}_{i}^{T} \boldsymbol{L}_{SC} \boldsymbol{\beta}_{i} \quad s.t. \quad \boldsymbol{\beta}_{i} \geq 0, \boldsymbol{\beta}_{i}^{T} \boldsymbol{1} = 1,$$
(2)

where,  $L_{SC}$  is the Laplacian matrix of the structural connectivity C with the i-th brain region excluded. The Laplacian matrix is defined as  $L_{SC} = D - C$ , where D is the degree matrix of structural connectivity. Since simplex constraint yield  $l_1$  penalty to be the constant term, we can rewrite eq. (2) as the following:

$$\tilde{\boldsymbol{\beta}}_{i} = \min_{\boldsymbol{\beta}_{\cdot}} ||\boldsymbol{X}_{(:,i)} - \boldsymbol{X}_{(:,\neq i)} \boldsymbol{\beta}_{i}||_{2}^{2} + \lambda_{G} \boldsymbol{\beta}_{i}^{T} \boldsymbol{L}_{SC} \boldsymbol{\beta}_{i} \quad s.t. \quad \boldsymbol{\beta}_{i} \geq 0, \boldsymbol{\beta}_{i}^{T} \boldsymbol{1} = 1.$$
 (3)

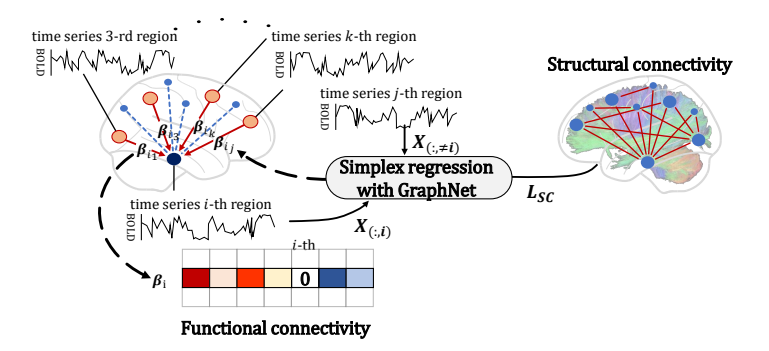


Fig. 1. The overall procedures of proposed algorithm.

The constraints in Eq. (3) is also simplex, so we can optimize it using the accelerated projected gradient method, as described in the next section.

We constructed the functional network by repeating the proposed algorithm p times for every brain region. The constructed network  $\mathbf{S} = [\widetilde{\boldsymbol{\beta}_1}, \widetilde{\boldsymbol{\beta}_2}, ..., \widetilde{\boldsymbol{\beta}_p}]$  is sparse and asymmetric. The  $\widetilde{\boldsymbol{\beta}_i}$  denoted a p dimensional vector, zero was inserted for the i-th coefficient of estimated coefficients vector  $\boldsymbol{\beta}_i$ . We defined the symmetric functional network by replacing  $\mathbf{S}_{(i,j)}$  and  $\mathbf{S}_{(j,i)}$  with the maximum value between them.

#### 3.3 Optimization details and the proposed algorithm

In this section, we describe an iterative algorithm for minimizing the cost function. The cost function, Eq. (3), can be solved by taking the derivative with respect to  $\beta_i$  and setting it to zero:

$$\boldsymbol{X}_{(:,\neq i)}^{T} \boldsymbol{X}_{(:,\neq i)} \boldsymbol{\beta}_{i} + \lambda_{G} \boldsymbol{L}_{SC} \boldsymbol{\beta}_{i} - \boldsymbol{X}_{(:,\neq i)}^{T} \boldsymbol{X}_{(:,i)} = 0.$$
(4)

Thus, the solution can be obtained by solving Eq. (4) as follows:

$$\tilde{\boldsymbol{\beta}}_{i} = \left(\boldsymbol{X}_{(:,\neq i)}^{T} \boldsymbol{X}_{(:,\neq i)} + \lambda_{G} \boldsymbol{L}_{SC}\right)^{-1} \boldsymbol{X}_{(:,\neq i)}^{T} \boldsymbol{X}_{(:,i)}.$$
 (5)

Next, we applied the accelerated projected gradient methods to solve the simplex problem as follow:

$$\min_{\beta_i} \frac{1}{2} ||\boldsymbol{\beta}_i - \boldsymbol{v}||_2^2 \quad s.t. \quad \boldsymbol{\beta}_i \ge 0, \boldsymbol{\beta}_i^T \mathbf{1} = 1,$$
 (6)

where  $\boldsymbol{v}$  denoted  $\tilde{\boldsymbol{\beta}}_i$ . We rewrite the Eq (6) using unconstrained formulation as

$$\frac{1}{2}||\boldsymbol{\beta}_i - \boldsymbol{v}||_2^2 - \gamma(\boldsymbol{\beta}_i^T \mathbf{1} - 1) - \boldsymbol{\lambda}^T \boldsymbol{\beta}_i, \tag{7}$$

where  $\gamma$  and  $\lambda$  is a Lagrangian multiplier and Lagrangian multiplier vector, respectively, both of which are to be determined. Suppose the optimal solution

to the proximal problem (6) is  $\beta^*$ , the associated Lagrangian multipliers are  $\gamma^*$  and  $\lambda^*$ . We then derived the following equations, according to the KKT conditions [1]:

$$\forall j, \boldsymbol{\beta}_{i_j}^* - \boldsymbol{v}_j - \gamma^* - \boldsymbol{\lambda}_j^* = 0, \tag{8}$$

$$\forall j, \boldsymbol{\beta}_{i_i}^* \ge 0, \tag{9}$$

$$\forall j, \boldsymbol{\lambda}_i^* \ge 0, \tag{10}$$

$$\forall j, \boldsymbol{\beta}_{i_j}^* \boldsymbol{\lambda}_j^* = 0, \tag{11}$$

where  $\boldsymbol{\beta}_{ij}^*$  denoted the j-th element of  $\boldsymbol{\beta}_i^*$ . We can rewrite Eq. (8) as  $\boldsymbol{\beta}_{ij}^* - \boldsymbol{v}_j - \gamma^* 1 - \boldsymbol{\lambda}_j^* = 0$ . We have  $\gamma^* = \frac{1 - \mathbf{1}^T \boldsymbol{v} - \mathbf{1}^T \boldsymbol{\lambda}^*}{n}$  using the constraint  $\boldsymbol{\beta}_i^T \mathbf{1} = 1$  and derive  $\boldsymbol{\beta}^* = \left(\boldsymbol{v} - \frac{1}{n} \mathbf{1}^T \boldsymbol{v} + \frac{1}{n} \mathbf{1} - \frac{\mathbf{1}^T \boldsymbol{\lambda}^*}{n} \mathbf{1}\right) + \boldsymbol{\lambda}^*$ . We rewrite it as  $\boldsymbol{\beta}^* = \boldsymbol{u} + \boldsymbol{\lambda}^* - \overline{\boldsymbol{\lambda}^*} \mathbf{1}$ , where  $\overline{\boldsymbol{\lambda}^*} = \frac{\mathbf{1}^T \boldsymbol{\lambda}^*}{n}$  and  $\boldsymbol{u} = \boldsymbol{v} - \frac{1}{n} \mathbf{1}^T \boldsymbol{v} + \frac{1}{n} \mathbf{1}$ . Thus,  $\forall j$  we have

$$\boldsymbol{\beta}_{i_j}^* = \boldsymbol{u}_j + \boldsymbol{\lambda}_j^* - \overline{\boldsymbol{\lambda}^*}. \tag{12}$$

According to Eqs. (9)-(12), we have  $\mathbf{u}_j + \mathbf{\lambda}_j^* - \overline{\lambda^*} = (\mathbf{u}_j - \overline{\lambda^*})_+$ , where  $x_+ = \max(x, 0)$ . We then have  $\boldsymbol{\beta}_{ij}^* = (\mathbf{u}_j - \overline{\lambda^*})_+$ . Therefore, given we know  $\overline{\lambda^*}$ , we can compute the optimal solution  $\boldsymbol{\beta}^*$ .

To obtain  $\overline{\lambda}^*$ , we rewrite Eq. (12) as  $\lambda_j^* = \overline{\lambda}^* + \beta_{i_j}^* - \boldsymbol{u}_j$ . According to Eqs. (9)-(11), we have  $\lambda_j^* = (\overline{\lambda}^* - \boldsymbol{u}_j)_+$ . Since  $\boldsymbol{v}$  is a p-1 dimensional vector, we have  $\overline{\lambda}^* = \frac{1}{p-1} \sum_{j=1}^{p-1} (\overline{\lambda}^* - \boldsymbol{u}_j)_+$ . Thus, we define a function as follow:

$$f(\overline{\lambda^*}) = \frac{1}{p-1} \sum_{j=1}^{p-1} (\overline{\lambda^*} - \boldsymbol{u}_j)_+ - \overline{\lambda}, \tag{13}$$

and we obtain  $\overline{\lambda^*}$  by solving Eq. (13) to be zero. Since  $\lambda^* \geq 0$ ,  $f'(\overline{\lambda^*}) \leq 0$ , and  $f'(\overline{\lambda^*})$  is a piecewise linear and convex function, we can compute the root of  $f'(\overline{\lambda^*}) = 0$  using Newton method efficiently.

### 4 Experiments and Results

### 4.1 Experimental results on Human Connectome Project data

In our experiments, we used pre-processed rs-fMRI and dMRI data, as described in Section 2.2. The rs-fMRI pre-processing procedure resulted in 2,400 time points for 372 regions, and the dMRI pre-processing yielded structural connectivity matrix (i.e.,  $372 \times 372$  matrix) based on probability tractography for each subject.

We applied the proposed model to construct functional networks. We compared our approach with five different functional network construction methods (i.e., PearC, PartC, GL, GL with structural connectivity [GLs], and simplex) according to previous studies [3, 9, 11]. When we constructed functional networks

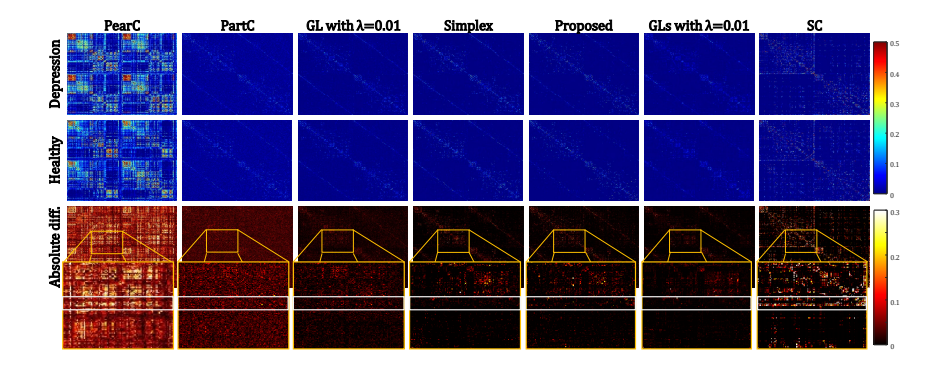
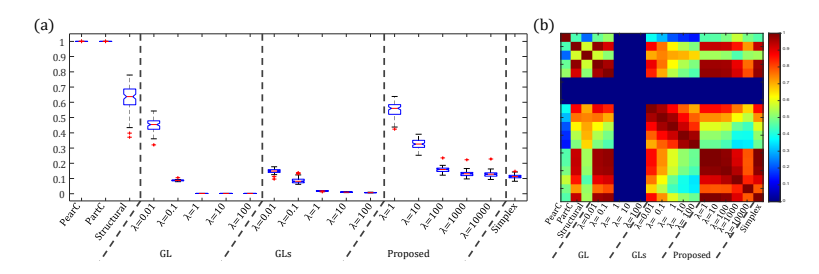


Fig. 2. Example of functional network map for each model. The first and second row are the functional network for depression and healthy group, respectively. The third row shows the absolute difference map between depression and healthy group. The fourth row shows an enlarged portion of each absolute difference map.



**Fig. 3. The sparsity and similarity comparison of networks.** Sub-figure (a) and (b) denoted a boxplot of the sparsity for each model and pair-wise correlation between models with varying hyper-parameters.

using our algorithm, GL, and GLs, we applied different sets of hyper-parameters for each model. We used [1, 10, 100, 1000, 10000] for the proposed algorithm, [0.01, 0.1, 1, 10, 100] for GL and GLs.

Overall, the constructed functional networks showed similar patterns except the PerC and SC, as shown in Fig. 2. We noted that our approach yielded more relevant and sparser patterns in sub-cortical structures compared to the methods using either fMRI and dMRI alone, as shown in the white box of Fig. 2. We compared the sparsity (ratio of non-zero connections in the functional network) for all methods. Fig. 3(a) shows the boxplots of sparsity across all subjects for each method. The sparsity decreased for every method, as we increase the hyperparameter value. For our approach, the sparsity did not change much when  $\lambda$  was larger than 100. The GL and GLs resulted in networks with almost zero sparsity, when  $\lambda$  was larger than 1. We also evaluated the similarity of the network patterns by reporting the pair-wise correlation among each method. We computed the correlation for network edge weights across subjects between two different methods (Fig. 3-(b)). Interestingly, the networks based on our approach

were very similar to those of partial correlation networks and the networks with GL. Finally, our results suggested that our approach constructed relatively sparse networks that are to some extent consist with existing methods but with better enriched sub-cortical structural connectivity information.

### 4.2 Evaluations using prediction task

In this section, we demonstrated and compared the efficacy of the constructed networks. However, there is no ground-truth for network constructions, thus we cannot directly compare the performances of all tested methods. Instead, we used the prediction task to compare the performances among different functional network construction methods. We first selected relevant features based on two-sample t-tests and built the ridge regression model to predict a DSM-dep score on the training set. A nested 10-fold-cross-validation was conducted to test the prediction performance. Specifically, the hyper-parameter for ridge regression was tuned using 10-fold-cross-validation on the training set. The trained prediction model was applied to testing set to measure the prediction performance.

After 10-fold-cross-validation, there were  $349.98 \pm 6.87$  features were selected with  $\lambda = 1000$ . The lowest root-mean-square-error (RMSE) of 3.783 was obtained using our algorithm with  $\lambda = 1000$ . Our algorithm also led to the highest correlation of 0.475 between the actual and predicted DSM5-Depression scores. Additionally, the GLs with  $\lambda = 0.01$  yielded a RMSE of 5.117 and a correlation of 0.279, the GL with  $\lambda = 0.01$  yielded a RMSE of 4.113 and correlation of 0.208, and the PartC yielded a RMSE 4.218 and correlation of 0.227. The detailed performances of seven different models with varying parameters were shown in Table 2. Interestingly, functional networks from GL and GLs with  $\lambda = 0.01$ , and our algorithm with  $\lambda = 1000$  showed similar network pattern and sparsity. However, our algorithm showed higher prediction performance than those from GL and GLs. Thus, we believe our approach leads to a more robust network with sparser connections.

**Table 2.** The prediction performances of various methods. Nested 10-fold-cross-validation was conducted to select the features and tune the hyper-parameters. The performance was reported in terms of RMSE and correlation coefficients (CC) between actual and predicted DSM-dep score. The asterisk denoted the CC with p < 0.05.

Method	RMSE	CC	Method	RMSE	CC
PearC	5.077	0.110	GLs $(\lambda = 1)$	5.252	-0.248*
PartC	4.218	0.227*	GLs $(\lambda = 10)$	-	-
$\operatorname{SC}$	4.597	0.139	$GL(\lambda = 100)$	-	-
$GL (\lambda = 0.01)$	4.113	0.208*	Ours $(\lambda = 1)$	4.799	0.119
$GL(\lambda = 0.1)$	5.153	-0.065	Ours $(\lambda = 10)$	4.557	0.261*
$GL(\lambda = 1)$	_	-	Ours $(\lambda = 100)$	4.191	0.240*
$GL(\lambda = 10)$	-	-	Ours $(\lambda = 1000)$	3.783	0.475*
$GL(\lambda = 100)$	-	-	Ours $(\lambda = 10000)$	4.119	0.232*
GLs ( $\lambda = 0.01$ )	5.117	0.279*	Simplex	4.548	0.110
GLs $(\lambda = 0.1)$	4.711	0.152			

### 5 Conclusion

In this work, we proposed a simplex regression model with GraphNet penalty to estimate functional networks enriched by structural connectivity. We demonstrated the feasibility of our algorithm on the HCP database. Compared to the existing methods, our model has two advantages. First, the functional network based on simplex regression can be interpreted as a probability, which can help further analysis. Second, the simplex representation with GraphNet can efficiently combine structural and functional information. Furthermore, we validated our proposed algorithm on real neuroimaging data and compared the results with those obtained using the existing competing methods.

In the future, we will further look into generating the whole-brain connectivity at once by applying the matrix optimization algorithm. Furthermore, there is no ground-truth for network constructions. Thus, our results should be further confirmed by future independent replications.

### References

- Boyd, S., Vandenberghe, L.: Convex Optimization. Cambridge University Press (2004)
- Damaraju, E., Allen, E., Belger, A., Ford, J., McEwen, S., Mathalon, D., Mueller, B., Pearlson, G., Potkin, S., Preda, A., Turner, J., Vaidya, J., van Erp, T., Calhoun, V.: Dynamic functional connectivity analysis reveals transient states of dysconnectivity in schizophrenia. NeuroImage: Clinical 5, 298 – 308 (2014)
- 3. Friedman, J., Hastie, T., Tibshirani, R.: Sparse inverse covariance estimation with the graphical lasso. Biostatistics 9(3), 432–441 (2008)
- 4. Glasser, M., C.T.R.E.e.a.: A multi-modal parcellation of human cerebral cortex. Nature **536**, 171–178 (2016)
- Glasser, M.F., Sotiropoulos, S.N., Wilson, J.A., Coalson, T.S., Fischl, B., Andersson, J.L., Xu, J., Jbabdi, S., Webster, M., Polimeni, J.R., et al.: The minimal preprocessing pipelines for the human connectome project. Neuroimage 80, 105–124 (2013)
- Grosenick, L., Klingenberg, B., Katovich, K., Knutson, B., Taylor, J.E.: Interpretable whole-brain prediction analysis with graphnet. NeuroImage 72, 304 321 (2013)
- 7. Huang, H., Yan, J., Nie, F., Huang, J., Cai, W., Saykin, A.J., Shen, L.: A new sparse simplex model for brain anatomical and genetic network analysis. In: International Conference on Medical Image Computing and Computer-Assisted Intervention. pp. 625–632 (2013)
- 8. Kim, M., Won, J.H., Youn, J., Park, H.: Joint-connectivity-based sparse canonical correlation analysis of imaging genetics for detecting biomarkers of parkinson's disease. IEEE Transactions on Medical Imaging 39(1), 23–34 (2020)
- Li, K., Guo, L., Nie, J., Li, G., Liu, T.: Review of methods for functional brain connectivity detection using fmri. Computerized Medical Imaging and Graphics 33(2), 131–139 (2009)
- Li, Y., Liu, J., Luo, M., Li, K., Yap, P.T., Kim, M., Wee, C.Y., Shen, D.: Structural connectivity guided sparse effective connectivity for mci identification. In: International Workshop on Machine Learning in Medical Imaging. pp. 299–306 (2017)

- Marrelec, G., Krainik, A., Duffau, H., Pélégrini-Issac, M., Lehéricy, S., Doyon, J., Benali, H.: Partial correlation for functional brain interactivity investigation in functional mri. Neuroimage 32(1), 228–237 (2006)
- Nedley, N., Ramirez, F.E.: Nedley depression hit hypothesis: identifying depression and its causes. American Journal of Lifestyle Medicine 10(6), 422–428 (2016)
- 13. Park, B.y., Seo, J., Park, H.: Functional brain networks associated with eating behaviors in obesity. Scientific reports 6(1), 1–8 (2016)
- Pervaiz, U., Vidaurre, D., Woolrich, M.W., Smith, S.M.: Optimising network modelling methods for fmri. NeuroImage 211, 116604 (2020)
- Pineda-Pardo, J.A., Bruña, R., Woolrich, M., Marcos, A., Nobre, A.C., Maestú, F., Vidaurre, D.: Guiding functional connectivity estimation by structural connectivity in meg: an application to discrimination of conditions of mild cognitive impairment. Neuroimage 101, 765–777 (2014)
- Rubinov, M., Sporns, O.: Complex network measures of brain connectivity: uses and interpretations. Neuroimage 52(3), 1059–1069 (2010)
- Salimi-Khorshidi, G., Douaud, G., Beckmann, C.F., Glasser, M.F., Griffanti, L., Smith, S.M.: Automatic denoising of functional mri data: combining independent component analysis and hierarchical fusion of classifiers. Neuroimage 90, 449–468 (2014)
- Smith, S.M., Jenkinson, M., Woolrich, M.W., Beckmann, C.F., Behrens, T.E., Johansen-Berg, H., Bannister, P.R., Luca, M.D., Drobnjak, I., Flitney, D.E., Niazy, R.K., Saunders, J., Vickers, J., Zhang, Y., Stefano, N.D., Brady, J.M., Matthews, P.M.: Advances in functional and structural mr image analysis and implementation as fsl. NeuroImage 23, S208 – S219 (2004)
- Smith, S.M., Miller, K.L., Salimi-Khorshidi, G., Webster, M., Beckmann, C.F., Nichols, T.E., Ramsey, J.D., Woolrich, M.W.: Network modelling methods for fmri. NeuroImage 54(2), 875 – 891 (2011)
- Stam, C.J., Jones, B., Nolte, G., Breakspear, M., Scheltens, P.: Small-world networks and functional connectivity in alzheimer's disease. Cerebral cortex 17(1), 92–99 (2007)
- 21. Wee, C.Y., Yap, P.T., Zhang, D., Denny, K., Browndyke, J.N., Potter, G.G., Welsh-Bohmer, K.A., Wang, L., Shen, D.: Identification of mci individuals using structural and functional connectivity networks. Neuroimage **59**(3), 2045–2056 (2012)
- 22. Werring, D., Clark, C., Barker, G., Miller, D., Parker, G., Brammer, M., Bullmore, E., Giampietro, V., Thompson, A.: The structural and functional mechanisms of motor recovery: complementary use of diffusion tensor and functional magnetic resonance imaging in a traumatic injury of the internal capsule. Journal of Neurology, Neurosurgery & Psychiatry 65(6), 863–869 (1998)
- 23. Zhang, Z., Liao, W., Chen, H., Mantini, D., Ding, J.R., Xu, Q., Wang, Z., Yuan, C., Chen, G., Jiao, Q., et al.: Altered functional–structural coupling of large-scale brain networks in idiopathic generalized epilepsy. Brain 134(10), 2912–2928 (2011)